Uncertainties in Ice-Sheet Altimetry From a Spaceborne 1064-nm Single-Channel Lidar Due to Undetected Thin Clouds

Yuekui Yang, Alexander Marshak, Tamás Várnai, Warren Wiscombe, and Ping Yang

***Abstract*—In support of the Ice, Cloud, and land Elevation Satellite (ICESat)-II mission, this paper studies the bias in surface-elevation measurements caused by undetected thin clouds. The ICESat-II satellite may only have a 1064-nm single-channel lidar onboard. Less sensitive to clouds than the 532-nm channel, the 1064-nm channel tends to miss thin clouds. Previous studies have demonstrated that scattering by cloud particles increases the photon-path length, thus resulting in biases in ice-sheet-elevation measurements from spaceborne lidars. This effect is referred to as atmospheric path delay. This paper complements previous studies in the following ways: First, atmospheric path delay is estimated over the ice sheets based on cloud statistics from the Geoscience Laser Altimeter System onboard ICESat and the Moderate Resolution Imaging Spectroradiometer (MODIS) onboard Terra and Aqua. Second, the effect of cloud particle size and shape is studied with the state-of-the-art phase functions developed for MODIS cirrus-cloud microphysical model. Third, the contribution of various orders of scattering events to the path delay is studied, and an analytical model of the first-order scattering contribution is developed. This paper focuses on the path delay as a function of telescope field of view (FOV). The results show that reducing telescope FOV can significantly reduce the expected path delay. As an example, the average path delays for $FOV = 167$ μrad (a 100-m-diameter circle on the surface) caused by thin undetected clouds by the 1064-nm channel over Greenland and East Antarctica are illustrated.**

***Index Terms*—Atmospheric path delay, Ice, Cloud, and land Elevation Satellite (ICESat)-II, lidar altimetry, polar cloud, radiative transfer.**

I. Introduction

SPACEBORNE lidars, such as the Geoscience Laser Altimeter System (GLAS) onboard the Ice, Cloud, and land Elevation Satellite (ICESat), provide measurements of ice sheets and sea ice on a global scale. These data are used to address important climate questions, such as "how is the cryosphere responding to the climate change?" and "how is the change in ice sheets affecting the global sea level?" [1]. To answer these questions, accurate ice-surface-elevation measurements are needed. The ICESat science objectives require detecting long-term elevation changes with an accuracy of < 1.5 cm/year over ice-sheet areas of 100×100 km^2 [1], [2].

Atmospheric factors, e.g., clouds, aerosols, and atmosphere humidity, may affect the accuracy of the derived ice surface elevation. Among these factors, clouds probably cause the most uncertainty due to the large variability in their properties. Clouds affect lidar measurements through particle forward scattering [3], which increases the photon-path length and makes the surface appear farther from the satellite. This effect is referred to as "atmospheric path delay." Some of the pioneering studies on this effect were reported by Duda *et al.* [2] and Mahesh *et al.* [4]. These studies demonstrated that the magnitude of the atmospheric path delay is a function of cloud height, cloud optical depth (COD, referred hereinafter as τ), cloud particle size and shape, and the telescope field of view (FOV). It was found that the delay could reach tens of centimeters even for optically thin clouds with a low cloud base.

The challenge in cloud-induced atmospheric path delay is twofold. First, if we know that the lidar beam hits a cloud, how do we correct the retrieved surface elevation? Second, if some clouds are not detected due to the low signal-to-noise ratio of the instrument, how large may the bias be in the altimetry products? Much progress has been made in addressing the first question [2], [4]. The second question is not a pressing issue for ICESat, because the GLAS lidar has two channels, one at 1064 nm and one at 532 nm. The 532-nm channel, used as the primary channel for GLAS atmospheric products, is very sensitive to the presence of clouds [5], [6]. It has been shown that cloud layers with an optical thickness as low as 0.01 generally were detectable with a well-functioning 532-nm laser channel [5]. However, the ICESat-II mission may only have the 1064-nm channel, and undetected clouds will become an important issue. It is critical to understand the probability that the 1064-nm channel may miss the detection of some clouds, and how the missed clouds may affect the altimetry measurements.

The ICESat-II mission is recommended by the National Research Council's Decadal Survey as one of the top-priority NASA missions [7]. However, without the 532-nm channel, its ability to detect clouds will be less than that of the current ICESat mission. Following [5], Fig. 1 shows this problem. The figure shows the percentage of the undetected clouds by

Manuscript received April 10, 2009; revised June 22, 2009. First published September 22, 2009; current version published December 23, 2009. This work was supported by National Aeronautics and Space Administration under the ICESat II Science Definition Project.

Y. Yang is with the Goddard Earth Science and Technology Center, University of Maryland, Baltimore County, Baltimore, MD 21228 USA (e-mail: yuekui.yang@nasa.gov).

A. Marshak and W. Wiscombe are with the NASA Goddard Space Flight Center, Greenbelt, MD 20771 USA (e-mail: Alexander.marshak@nasa.gov; warren.j.wiscombe@nasa.gov).

T. Várnai is with the Joint Center for Earth Systems Technology of the University of Maryland, Baltimore County, Baltimore, MD 21228 USA, and of the NASA Goddard Space Flight Center, Greenbelt, MD 20771 USA (e-mail: tamas.varnai@nasa.gov).

P. Yang is with the Department of Atmospheric Sciences, Texas A&M University, College Station, TX 77843 USA (e-mail: pyang@ariel.met.tamu.edu).

Digital Object Identifier 10.1109/TGRS.2009.2028335

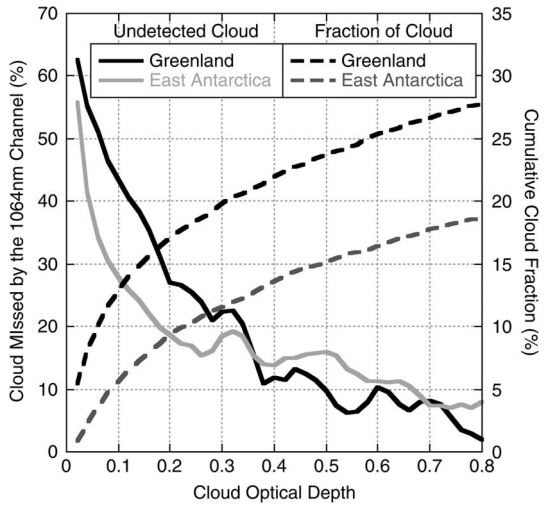

Fig. 1. Probability of a cloud being missed by the 1064-nm channel when compared to the cloud-detection results of the 532-nm channel as a function of COD and the cumulative cloud fraction, as detected by the 532-nm channel for Greenland and East Antarctica. Fraction of cloud with a given optical depth is defined as the frequency of occurrence of clouds out of the total number of observations. Data are the 1-Hz product from the GLAS L2A campaign (September 25 to November 19, 2003).

the 1064-nm channel, compared to the cloud-detection results by the 532-nm channel. The data are the 1-Hz products from the GLAS campaign conducted from September 25 to November 19, 2003 (termed L2A) [5], [6], [8]. As shown in the figure, 43% of clouds with an optical depth of 0.1 were undetected by the 1064-nm channel over Greenland and 29% over East Antarctica. For clouds with an optical depth of 0.2, 27% of clouds over Greenland and 19% over East Antarctica were undetected. In addition, shown in Fig. 1 is the cumulative cloud fraction, defined as the frequency of occurrence of clouds with optical depth smaller than a certain value out of the total number of observations (cloudy and clear). The cumulative cloud fraction shows how often clouds within certain optical depth range occur. For example, the fraction of clouds with optical depth smaller than 0.2 is 17% over Greenland and 9% over East Antarctica. Calculations show that, during the L2A period, the total cloud fractions are 60% and 34% over Greenland and East Antarctica, respectively (not shown). It should be pointed out that during the L2A campaign, most of the observations over Greenland and East Antarctica were conducted during nighttime and daytime, respectively. Over Greenland, there was less interference from solar background radiances and more thin clouds were detected than over East Antarctica.

Using cloud properties observed by GLAS and Moderate Resolution Imaging Spectroradiometer (MODIS), this paper will address two main questions in support of the ICESat-II mission: 1) what is the expected delay caused by the undetected clouds as a function of telescope FOV? and 2) how small the FOV must be to meet the science requirement? This paper is organized as follows. Section II gives a review of how different cloud properties affect atmospheric path delay with a focus on the cloud particle-phase function. In Section III, we discuss the contributions of different orders of scattering to the delay. Section IV conducts a cloud-detectability comparison between the 532-nm and the 1064-nm channels. Statistics of the properties of the thin clouds that the 1064-nm channel fails to detect are presented in Section V. Section VI estimates the average atmospheric path delay resulting from the undetected clouds. The conclusions of this paper are discussed in Section VII. An analytical model for the path delay caused by single scattering is presented in the Appendix.

II. Parameters Affecting Atmospheric Path Delay

In this paper, simulations are conducted with our 3-D radiative-transfer Monte Carlo model [9] that has been validated by the International 3-D Radiation Code project [10]. Lidar pulses are assumed to be the Dirac-delta function. The shape of the lidar pulse does not affect our results, because atmospheric path delay is calculated as an average value of the delays experienced by individual photons. It should be pointed out that the surface-altitude bias is one half of the path delay. In the simulations, clouds are assumed to be horizontally and vertically homogenous. Since we focus on thin clouds over polar ice sheets, the cloud particle phase is presumed to be ice.

Cloud properties, e.g., height, optical depth, and particle size and shape, are essential to the determination of atmospheric path delay [2]. Fig. 2 shows some examples of the effect that different parameters have on path delay. Fig. 2(a) shows atmospheric path delay as a function of the cloud base height for clouds of two different optical depths (0.1 and 0.2) and two FOVs (475 and 167 μrad). The 475 μrad, which translates to a 285-m-diameter circle on the surface for the 600-km orbital altitude of the satellite, is the FOV of the current ICESat; 167 μrad, which corresponds to a 100-m-diameter circle on the surface, is the proposed FOV of ICESat-II [11]. In general, photons scattered by low clouds experience longer paths inside the telescope FOV than the ones scattered by high clouds; hence, path delay generally decreases as cloud base height increases. However, the path delay is not always a monotonic function of cloud base height. Rather, it is a cumulative result of several factors (refer to the Appendix), including phase function, maximum scattering angle, and COD. It should be noted that the effect of cloud geometrical thickness acts collaboratively with cloud base height. For clouds with the same base height, the thicker the cloud, the higher is the equivalent cloud altitude. Obviously, COD is another important factor in the determination of path delay. A larger optical depth means higher probability of photons being scattered, thus causing a larger path delay.

Fig. 2(b) shows the effect of cloud particle-phase functions and telescope FOV on atmospheric path delay. Simulations were conducted for a variety of phase functions, including the phase function adopted by the MODIS ice-cloud property retrievals (see [12] and [13] for details); the phase functions associated with nonspherical particle shapes such as hollow columns, plates, and spheres [13]; and the isotropic phase function. The results show that particle-phase function is an important factor, particularly for large FOVs. Moreover, the path delay is essentially a forward-scattering issue as can be seen that, for the isotropic phase function, the delay is much smaller and practically negligible for $FOV < 300$ μrad as compared to the results from other phase functions. Additionally, the size of the telescope FOV is another important factor that affects path-delay determination. The larger the FOV, the higher is the probability of multiple scattered photons reaching the sensor;

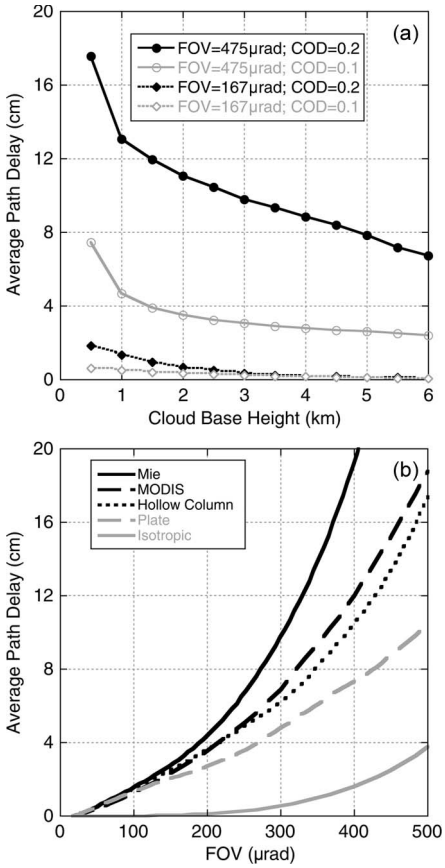

Fig. 2. Examples of parameters affecting atmospheric path delay. (a) Path delay as a function of cloud base height for clouds of two different optical depths (0.1 and 0.2) and two different FOVs (167 and 475 μrad). Cloud geometrical thickness is 500 m. MODIS ice phase function for $r_e = 20$ μm used. (b) Path delay as a function of the telescope FOV for different particle shapes. Cloud base height is 500 m; cloud geometrical thickness is 500 m; $\tau = 0.2$; $r_e = 20$ μm. Isotropic phase function is added for illustrative purposes.

hence, reducing the FOV could reduce path delay substantially. For example, for the current ICESat FOV (475 μrad), a cloud with an optical depth of 0.2, a base height of 0.5 km, and a geometrical thickness of 0.5 km will cause a path delay of about 16 cm (for the MODIS phase function and $r_e = 20$ μm). However, if the FOV is reduced to 167 μrad, the path delay for the same cloud is reduced to 2.5 cm.

III. Contribution of Different Orders of Scattering

To further understand the mechanism of atmospheric path delay, we separate the results into contributions from different orders of scattering. Fig. 3 shows these contributions, as a function of FOV, for CODs of 0.05, 0.1, and 0.2. In the figure, the scattering number is the accumulated times that a photon is scattered within a cloud. For example, first-order scattering means the photon is only scattered once in the cloud, which can happen either on the downward path to the surface or on the upward path to the sensor. Obviously, the thicker the cloud, the more important is multiple scattering. For the case shown in this paper, if $\tau = 0.05$, the contribution from single-order scattering is about 95%; if $\tau = 0.1$, the contribution is about 90%; and if $\tau = 0.2$, the contribution is about 80%. Generally,

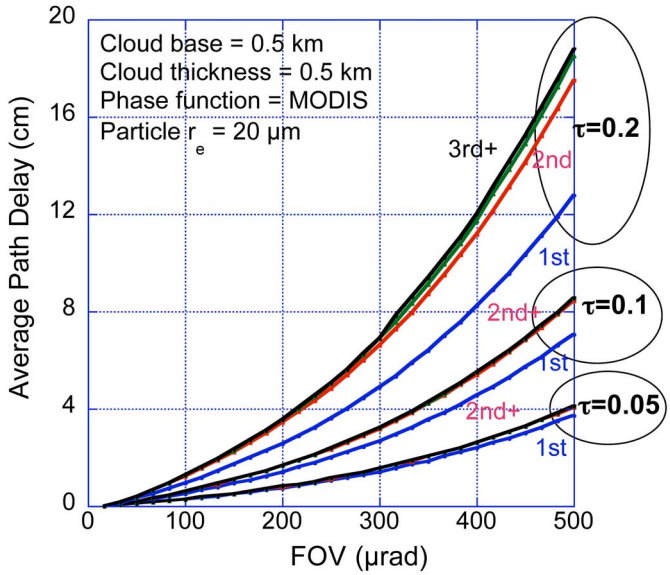

Fig. 3. Path-delay contributions from different orders of scattering as a function of FOV: for $\tau = 0.05$, 0.1, and 0.2; cloud at 0.5–1.0 km; $r_e = 20$ μm; MODIS ice phase function used. Blue, red, green, and black lines illustrate cases when up to first, second, third, and all orders of scattering are taken into account, respectively.

for thin clouds, results from first-order scattering gives a good approximation to path delay, particularly for small FOVs.

The path delay resulting from first-order scattering can be calculated analytically. We present the derivation and validation of an analytical model for first-order-scattering-induced path delay in the Appendix. A model that includes second-order scattering will be presented in a follow-up study.

Fig. 4(a) shows how the lidar backscattering and path delay are distributed among different orders of scattering for two FOVs: 475 and 167 μrad. Since the cloud is thin ($\tau = 0.1$), the lidar signal is dominated by the nonscattered photons. In this case, about 90% of the lidar returned signal is from nonscattered photons and about 10% is from photons being scattered once within the cloud. As expected, the plot also shows that, for the larger FOV, multiple scattering contributes more to both the backscattering signal and the path delay. Fig. 4(b) shows the probability of photons being scattered up to a given scattering angle for a variety of particle shapes. As expected from diffraction theory (e.g., [3]), about 50% of all photons are scattered into a narrow forward-scattering peak.

For first-order scattering, the maximum scattering angle for a photon to stay in the FOV can be calculated as (see the Appendix)

$$\theta_s = \arctan\left(\frac{f \times 10^{-6} \times h}{2z}\right) \tag{1}$$

where $h = 6 * 10^6$ m (satellite orbital height), f is the FOV in microradians, and z is the cloud altitude in meters.

For cloud altitudes between 500 and 6000 m and for 100 μrad $\leq$ FOV $\leq$ 500 μrad, the maximum scattering angle ranges from 0.5° to 15°. The lidar return from zeroth-order scattering and first-order scattering can be approximately expressed as follows: $(1/1+\tau) \times 100\%$ and $(\tau/1+\tau) \times 100\%$ (see the Appendix for details). For $\tau = 0.1$, calculations show

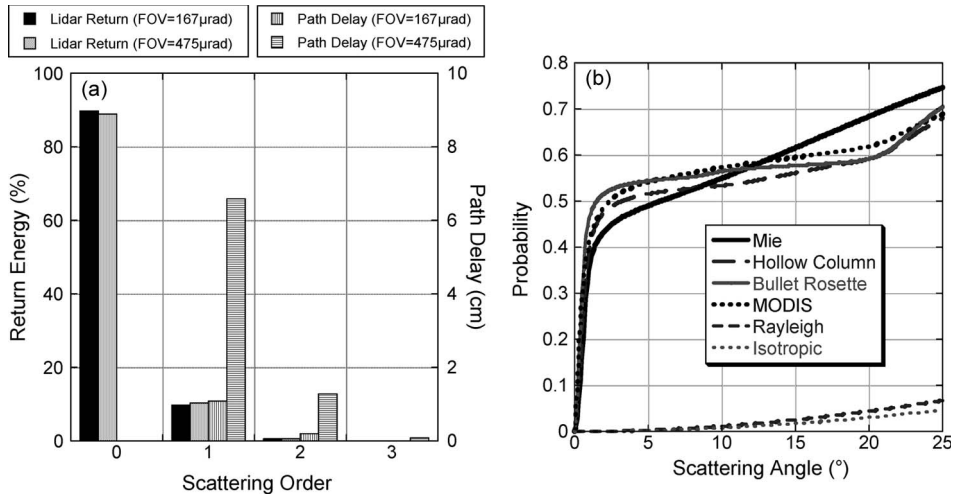

Fig. 4. (a) Monte Carlo simulated results of contributions to both lidar return and path delay from different orders of scattering for two FOVs: 475 and 167 μrad with COD 0.1. Cloud base height is 500 m; cloud geometrical thickness is 1000 m; MODIS phase function used; $r_e = 20$ μm. (b) Phase function integrals of different particle shapes, which give the probability of photons being scattered within the scattering angle. Phase functions of Mie, Hollow Column, Bullet Rosette, and MODIS are for $r_e = 20$ μm. Rayleigh and isotropic phase functions are included for illustrative purposes.

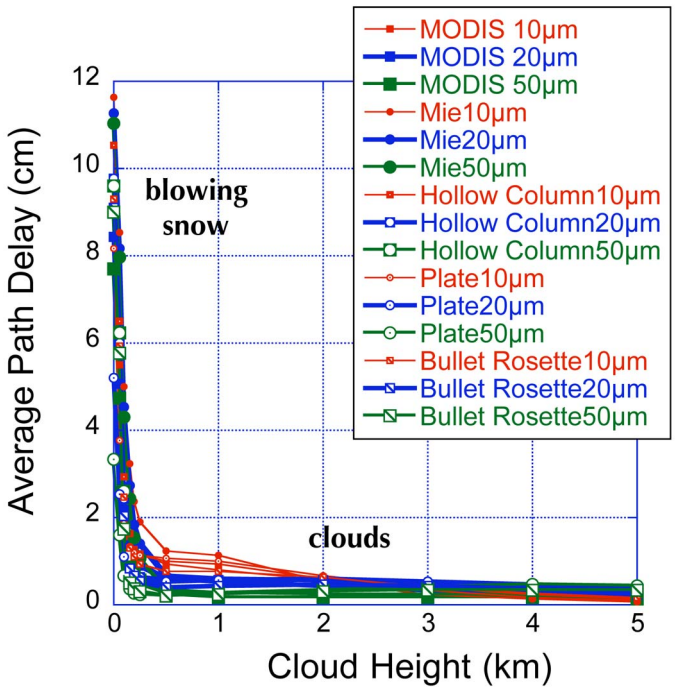

Fig. 5. Path delay as a function of scattering layer altitude and particle shape for COD of 0.05. $FOV = 167$ μrad. Calculated with the analytical model presented in the Appendix.

that photons without any scattering account for 91% of the lidar returns and photons being scattered once account for 9%. These numbers match the Monte Carlo results.

The aforementioned simulations apply only to clouds. Blowing snow is another factor that could potentially cause large path delays over polar ice sheets. Fig. 5 shows path-delay calculations using the analytical model given in the Appendix. The optical depth is assumed to be 0.05, so the first-order scattering approximation is applicable. As shown in the figure, even a thin layer of blowing snow ($\tau = 0.05$) can ensue a large path delay (over 10 cm for some particle shapes). However, this paper will only focus on path delays resulting from clouds. The effect of blowing snow needs further investigation and will be addressed in our future studies.

IV. Cloud Detectability Comparison Between the 532-nm and the 1064-nm Channels

As aforementioned in Section I, it is critical for the ICESat-II mission to understand what fraction of thin clouds would be missed by a single 1064-nm-channel lidar and what path delay the undetected clouds would cause. To investigate the capability differences in detecting thin clouds between the 532- and 1064-nm laser channels, we use the data from the GLAS campaign L2A. As aforementioned in Section I, L2A, which is the first GLAS campaign with full on-orbit operation of the instrument, began on September 25 and lasted until November 19, 2003. The GLAS cloud retrievals are archived in the products GLA09, global cloud heights for multilayer clouds, and GLA11, global thin cloud/aerosol optical-depth data [14]. The data used here are the 1-Hz cloud-property retrievals.

Fig. 6 shows the results for Greenland and East Antarctica. East Antarctica and West Antarctica are divided along the traditional boundary, the Transantarctic Mountains [15]. Similar to [5, Fig. 4], Fig. 6 shows the frequency distribution of GLAS CODs retrieved using the 532-nm-channel observations together with the frequency that the1064-nm channel flagged as cloudy for the corresponding optical depths. In addition, Fig. 6 shows the cumulative distribution of thin clouds missed by the 1064-nm channel, defined as the frequency of missed clouds out of all the transparent clouds detected by the 532-nm channel. Transparent clouds are clouds thin enough for GLAS to have ground return. We see that about 31% of all the transparent clouds were not detected by the 1064-nm channel over Greenland [Fig. 6(a)] and 22% over East Antarctica [Fig. 6(b)]. Undetected clouds are primarily thin clouds with $\tau < 0.2$. It is shown in Fig. 7 that, for clouds with $\tau < 0.2$ [Fig. 7(a)], the difference between cloud-detection results of the 1064-nm channel and the 532-nm channel is significant; yet for clouds with $\tau > 1.0$, both channels give similar results [Fig. 7(b)].

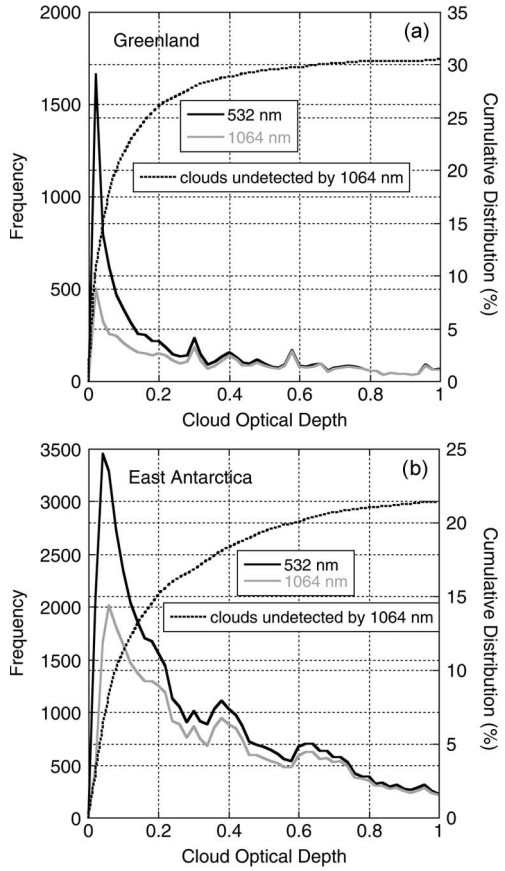

Fig. 6. Frequency of COD retrieved from (black line) the GLAS 532-nm channel together with clouds detected by (gray line) the 1064-nm channel; the dotted line is the cumulative distribution of thin clouds missed by the 1064-nm channel, defined as the frequency of missed clouds out of all transparent clouds detected by the 532-nm channel. Transparent clouds are clouds thin enough for GLAS to have ground return. Based on the 1-Hz data of GLAS L2A campaign for (a) Greenland and (b) East Antarctica (compare with [5, Fig. 4]).

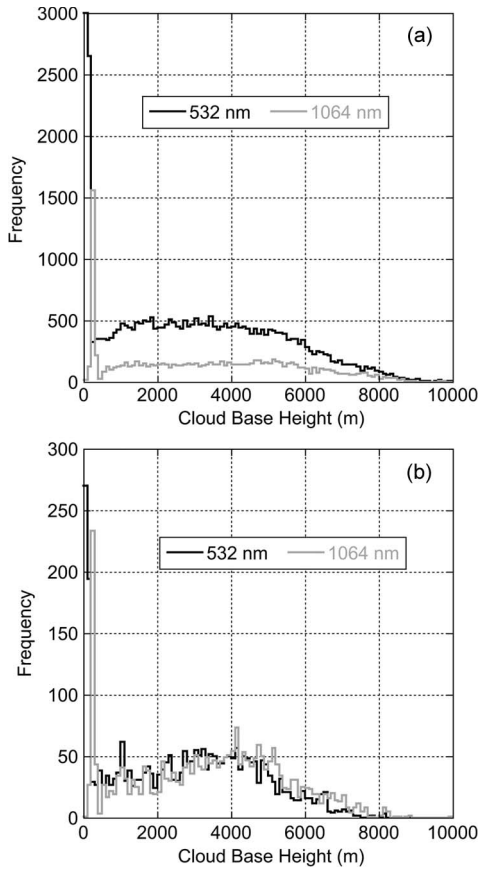

Fig. 7. Frequency of cloud base height retrieved from (black line) the GLAS 532-nm channel and (gray line) the 1064-nm channel. Based on the GLAS L2A campaign for East Antarctica for clouds with (a) $\tau \leq 0.2$ and (b) $1.0 \leq \tau \leq 2.0$.

It should be noted that the ability of the 1064-nm channel to detect thin clouds is a function of a variety of factors, such as atmospheric conditions, laser power, and algorithm. In this paper, we used the laser onboard the current ICESat as a benchmark.

V. Properties of Thin Clouds Observed by ICESat and MODIS Over Ice Sheets

As discussed in Section II, the atmospheric path delay strongly depends on cloud geometrical, optical, and microphysical properties [2]. To achieve a realistic estimate of the magnitude of delays caused by clouds missed by the 1064-nm channel, the following parameters are needed as input to our radiative-transfer model: cloud base height, cloud geometrical thickness, COD, and cloud particle size and shape. Studies, such as [16]–[18], have been conducted with ground-based measurements and *in situ* measurements. *In situ* and ground-based measurements are desirable in understanding polar-cloud microphysics, but they are rare in the polar regions, particularly in Antarctica. Spaceborne lidars such as GLAS [14] and Cloud-Aerosol Lidar with Orthogonal Polarization [19] provide a unique collection of data, and studies with these data have provided new insight into polar-cloud properties (e.g., [5], [8], and [20]).

In this paper, the distributions of cloud base height and COD are derived from the GLAS L2A campaign data set. Because cloud geometrical thickness acts collaboratively with cloud base height, it is not treated as an independent variable. In the following calculations, we assume that clouds are 500 m thick. Cloud thickness distributions (not shown) calculated from GLAS L2A peak at around 500 m. Fig. 8(a) shows the 2-D histogram of cloud base height versus COD for $\tau \leq 0.2$. These clouds are the focus of this paper, because they are the ones that the 1064-nm channel tends to miss.

In addition to COD, cloud base height, and cloud geometrical thickness, path-delay simulations require the phase function of the cloud particles, or equivalently, particle size and shape. Ice cloud particles are a mixture of different habits, and the determination of their phase functions is a complicated task [24]. Based on the ground-based observations around South Pole, Lawson *et al.* [18] reported that, of the all crystals observed, 30% were rosette shapes (mixed-habit rosettes, platelike polycrystals, and rosette shapes with side planes), 45% were diamond dust shapes (columns, thick plates, and plates), and 25% were irregular shapes. However, phase functions based on these observations are not readily available. In this paper, we adopt the MODIS cirrus-cloud microphysical model [12]. When the effective radius r_e is small ($r_e < 35$ μm), the habit mixture is prescribed as 50% bullet rosettes, 25% hexagonal plates, and 25% hollow columns. When $r_e \geq 35$ μm, the habit mixture is 30% aggregates, 30% bullet rosettes, 20% hexagonal

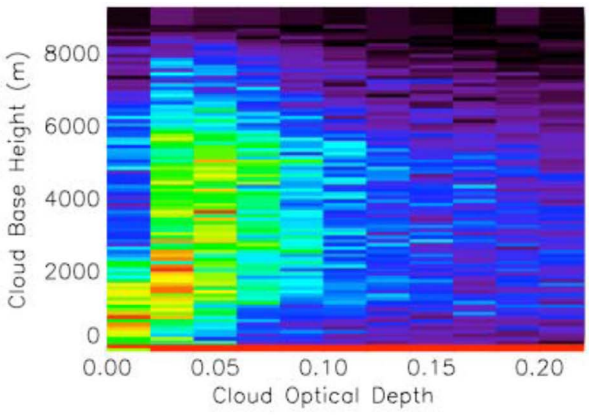

(a)

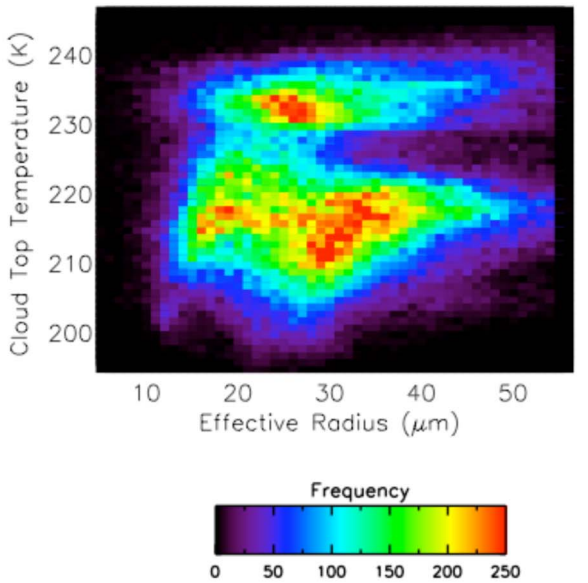

(b)

Fig. 8. Two-dimensional histograms for (a) GLAS COD versus cloud base height for clouds with $\tau \leq 0.2$ over East Antarctica. Data are from the GLAS L2A campaign. (b) MODIS cloud top temperature versus ice particle effective radius over East Antarctica. Data are from MODIS Aqua and Terra for the fall of 2003 (the time period as for the GLAS L2A campaign).

plates, and 20% hollow columns. As shown in Fig. 8(b), the MODIS-retrieved particle effective radii vary from 10 to 50 μm. MODIS retrievals over the polar regions have certain limitations. Due to the strong shortwave reflectance and the low thermal brightness temperature of the surface, it is more difficult for passive remote-sensing techniques to separate cloudy and cloud-free areas (e.g., [25] and [26]). Hence, the retrievals of COD and particle effective radius over these regions may have large uncertainties [21].

VI. Estimated Path Delay Over Ice Sheets

Based on the statistics presented in Sections IV and V, we are able to estimate the path delay resulting from the clouds missed by the 1064-nm-channel analysis as a function of telescope FOV. To do this, we calculate the average path delay as an integral

$$I(\Delta\psi) = \iiint p_{\text{missed}}(\tau)p(\tau, h_b, r_e) \times L(\tau, h_b, r_e; \Delta\psi)d\tau dh_b dr_e \quad (2)$$

where $\Delta\psi$ is the telescope FOV; $p_{\text{missed}}(\tau)$ is the probability density function (pdf) of clouds with optical depth τ being missed by the 1064-nm channel due to the lower signal-to-noise ratio; $p(\tau, h_{\text{b}}, r_e)$ is the pdf of clouds with optical depth τ, base height h_{b} (relative to surface elevation), and particle effective radius r_e; and $L(\tau, h_{\text{b}}, r_e; \Delta\psi)$ is the Monte Carlo calculated path delay as a function of $\Delta\psi$ for each combination of τ, r_e, and h_{b}.

Even though there is a known correlation between ice particle size and cloud temperature [22], our analysis of thin polar clouds observed by GLAS and MODIS does not show any pronounced correlation between cloud base height, COD, and cloud particle effective radius (Fig. 8). As a first approximation, we can consider these three variables independent from each other. Thus, (2) can be rewritten as

$$I(\Delta\psi) = \iiint p_1(\tau)p_2(h_b)p_3(r_e)L(\tau, h_b, r_e; \Delta\psi)\, d\tau dh_b dr_e \quad (3)$$

where $p_1(\tau) = p_{\text{missed}}(\tau)p(\tau)$ is the pdf of the clouds with optical depth τ undetected by the 1064-nm channel, $p_2(h_{\text{b}})$ is the pdf of cloud base height h_b, and $p_3(r_e)$ is the pdf of particle effective radius r_e.

The values of the distributions of COD, cloud effective radius, and cloud base height over Greenland and East Antarctica used in the calculation of average path delays are shown in Table I. The results on the expected path delay caused by the missed clouds as a function of telescope FOV is shown in Fig. 9. The error bars give the standard deviation of the path-delay calculations for different cloud base heights, CODs, and cloud particle effective radii. If the FOV is kept the same as the current ICESat, then over Greenland and East Antarctica, the bias would be 4.7 $\pm$ 4.0 and 4.3 $\pm$ 3.9 cm, respectively. Reducing the telescope FOV can significantly reduce the bias. If the FOV is reduced to 167 μrad, path delay will be around 0.9 $\pm$ 0.7 cm over Greenland and 0.8 $\pm$ 0.7 cm over East Antarctica.

We emphasize in this paper four important points: 1) the above values of path delay are not weighted with the total number of surface-elevation retrievals; 2) the fractions of undetected clouds are calculated based on the GLAS COD product, which is 1 Hz, while surface-elevation retrievals are on a 40-Hz basis; 3) blowing snow is not accounted; and 4) finally, to investigate the impact of undetected clouds on the long-term trend of ice-sheet elevation, we need to take into account the annual variability of the properties of the these clouds.

Let us briefly discuss the first two points. For simplicity, we assume that the total number of surface-elevation retrievals is equal to the total number of clear pixels as determined by the 1064-nm channel. Then, we can estimate the fraction of cloudy pixels misclassified as clear. Our calculations show that during the L2A campaign, the clear-sky fractions over Greenland were 40% and 46% and over East Antarctica were 66% and 72%,

TABLE I
PDF OF CLOUDS POTENTIALLY MISSED BY THE 1064-nm CHANNEL USED IN ESTIMATING AVERAGE PATH DELAYS OVER GREENLAND AND ANTARCTICA. IN THE TABLE, EA STANDS FOR EAST ANTARCTICA AND GL STANDS FOR GREENLAND

Cloud Optical Depth			Effective Radius			Cloud Base Height		
Value	PDF GL	PDF EA	Value (μm)	PDF GL	PDF EA	Value (m)	PDF GL	PDF EA
0.05	0.45	0.39	10	0.19	0.07	500	0.17	0.19
0.1	0.24	0.25	20	0.61	0.31	1000	0.20	0.21
0.15	0.15	0.17	30	0.15	0.32	2000	0.23	0.22
0.2	0.1	0.11	40	0.04	0.20	3000	0.21	0.19
0.25	0.06	0.08	50	0.01	0.10	4000	0.19	0.19

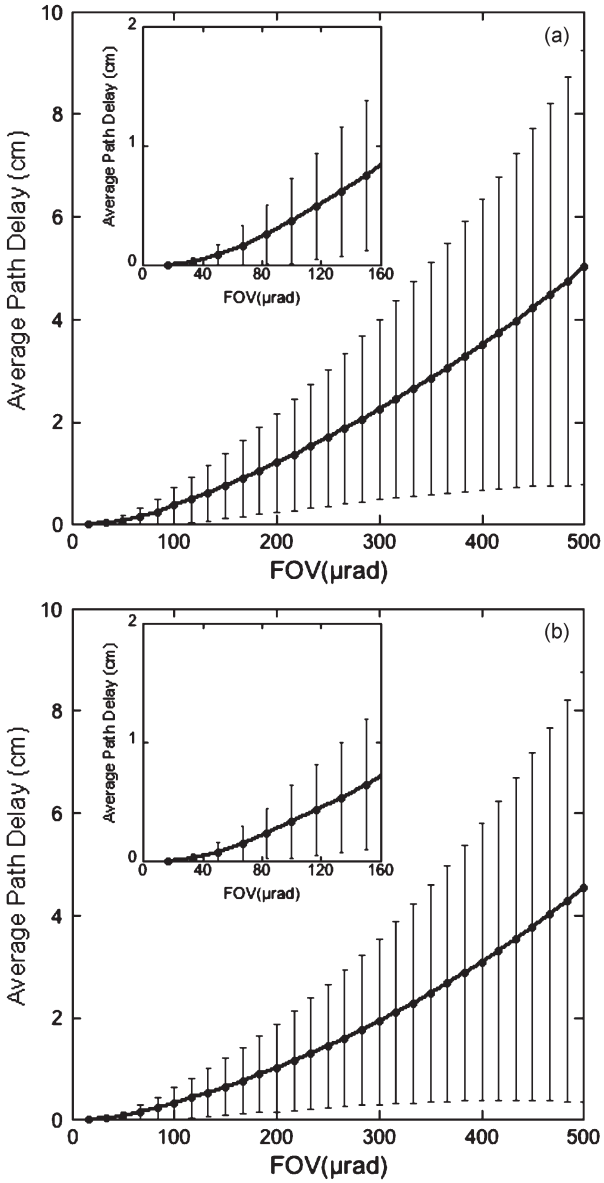

Fig. 9. Estimated average path delay resulting from clouds missed by the 1064-nm channel for 1-Hz data. Blowing snow is not included. (a) Greenland. (b) East Antarctica. Insets are the zoomed-in version for smaller FOVs.

for the 532- and 1064-nm channels, respectively. Hence, the fraction of misclassified clouds is $(46-40)/46=13\%$ over Greenland and $(72-66)/72=8\%$ over East Antarctica. Calculations show similar results for smaller Antarctic regions, e.g., Pine Island, Lake Vostok, and Interior West Antarctica. To summarize, roughly 10% of all laser shots identified by the 1064-nm channel as clear are actually misclassified cloudy shots that result in range delay. Thus, our estimated average path delay due to undetected clouds has to be reduced by a factor of ten.

It is important to note that the earlier results are for the 1-Hz data. Since the 40-Hz data are used for surface-elevation retrievals, we need to understand the 40-Hz range delay as well. In general, it is not a straightforward problem because the 532-nm channel does not provide retrievals of COD at 40 Hz. However, with some simplified assumptions, range delay for 40 Hz can be estimated based on the 1-Hz estimates. If we assume constant signal, then averaging over 40 (independent) data points will increase the signal-to-noise ratio by a factor of $\sqrt{40}=6.3$. If we further assume that for optically thin clouds the backscatter signal is proportional to COD, then the optically thicker clouds will be undetected at 40 Hz as likely as their 6.3 times thinner counterparts at 1 Hz. Next, since, for thin clouds, the photon path delay and COD is approximately linearly related (see Fig. 3), then the average path delay would be also 6.3 times larger.

VII. SUMMARY AND DISCUSSION

Duda *et al.* [2] showed that atmospheric path delay is sensitive to cloud height, COD, ice particle-phase functions, and the telescope FOV. This paper complements [2] in three ways: 1) Atmospheric path delay due to thin clouds missed by the 1064-nm channel is determined using cloud observations by GLAS and MODIS; 2) the state-of-the-art models of scattering phase functions were used, and the effect of cloud particle size and shape on atmospheric path delay has been studied; 3) contributions to the path delay from different orders of scattering have been estimated. For very thin clouds missed by the 1064-nm channel, the single-scattering approximation is found to be accurate enough, and an analytical path-delay model has been developed for this case. The major findings of this paper can be summarized as follows.

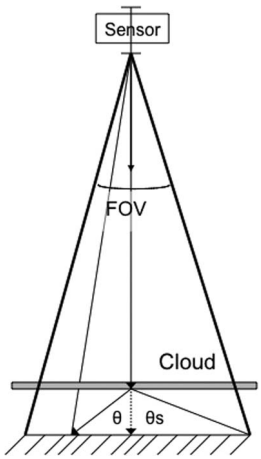

Fig. 10. Schematic picture of path delay caused by forward scattering. Solid arrow lines represent the path of scattered photons. Dashed arrow line represents the path of nonscattered photons. θ is the scattering angle, and $\theta_{\rm s}$ is the largest possible scattering angle for a photon to stay in the FOV.

Path delay is strongly affected by the forward-scattering peak of the cloud particle-phase function or, equivalently, the size and shape of the particles. However, the phase-function effect substantially decreases with a reduction in the telescope FOV.

As a first-order approximation, atmospheric path delay can be calculated from a simple analytical formula. This formula, accounting for the delay caused by first-order scattering photons, provides an efficient way to estimate the delay resulting from very thin clouds.

The 1064-nm channel alone tends to miss very thin clouds. According to the 1-Hz GLAS products, this channel fails to record about 20%–30% of the transparent clouds. The majority of the undetected clouds have $\tau \leq 0.2$.

Calculations of the expected path delay resulting from undetected clouds (so-called the residual bias) using GLAS and MODIS data show that reducing telescope FOV from 475 (current ICESat) to 167 μrad (proposed for ICESat-II) will substantially mitigate the problem. The expected mean path delay due to undetected clouds for 167-μrad FOV and the 40-Hz data found to be smaller than 1 cm. However, since the ICESat-II orbit will follow a 91-day repeat cycle that provides only four measurements at a given point each year, the low rate of sampling requires accounting not only for the expected average bias but also for the maximum possible errors. In addition, the effect of blowing snow, which could potentially cause larger delay, is not considered in this paper and will be reported separately.

APPENDIX
SIMPLE ANALYTICAL MODEL FOR ATMOSPHERIC PATH DELAY CAUSED BY SINGLE SCATTERING IN CLOUDS

In this section, we derive a simple analytical model for atmospheric path delay caused by first-order scattering. This model provides an efficient way to estimate path delays due to very thin clouds. A more complicated model that includes second-order scattering will be investigated in a follow-up study.

From Fig. 10, for photons scattered at angle θ, the path delay can be calculated as [2]

$$\Delta(z,\theta) = \frac{z}{\cos(\theta)} z. \tag{A1}$$

Let us only consider the range delay caused by photons experiencing single scattering, which could happen either on the downward path to surface or on the upward path to the sensor. The probability of photons being scattered once within a cloud of optical depth τ can be written as (see, e.g., [23, p. 219])

$$p_1 = \tau e^{-\tau}. \tag{A2}$$

Assuming a Lambertian surface with albedo $\alpha_{\rm s}$, the total delay resulting from photons scattered once on the down/up path and unscattered on the up/down path is

$$\left[\tau e^{-\tau}\left(\frac{1}{2}\int_0^{\theta_s}\Delta(z,\theta)P(\theta)\sin(\theta)d\theta\right)\right]\alpha_s e^{-\tau}$$

$$= \alpha_s \tau e^{-2\tau}\left(\frac{1}{2}\int_0^{\theta_s}\Delta(z,\theta)P(\theta)\sin(\theta)d\theta\right) \tag{A3}$$

where θ_s is the largest possible scattering angle for a photon to stay in the FOV and $P(\theta)$ is the scattering phase function normalized as

$$\frac{1}{2}\int_0^{\pi} P(\theta)\sin(\theta)d\theta = 1. \tag{A4}$$

Given satellite orbital altitude h (in meters), cloud height z (in meters), and telescope FOV f (in microradians), θ_s can be calculated as follows:

$$\theta_s = \arctan\left(\frac{f\times 10^{-6}\times h}{2z}\right). \tag{A5}$$

The probability of photons reaching the sensor without being scattered within the cloud is

$$S_0 = \alpha_s e^{-2\tau}. \tag{A6}$$

The probability of photons reaching the sensor being scattered once within the cloud is

$$S_1 = 2\alpha_s \tau e^{-2\tau}\left(\frac{1}{2}\int_0^{\theta_s} P(\theta)\sin(\theta)d\theta\right). \tag{A7}$$

Hence, the average delay caused by the photons being scattered once can be calculated as

$$\overline{\Delta} = \frac{2\alpha_s\tau e^{-2\tau}\left(\frac{1}{2}\int_0^{\theta_s}\Delta(z,\theta)P(\theta)\sin(\theta)d\theta\right)}{\alpha_s e^{-2\tau} + 2\alpha_s\tau e^{-2\tau}\left(\frac{1}{2}\int_0^{\theta_s} P(\theta)\sin(\theta)d\theta\right)}$$

$$= \frac{\tau\left(\int_0^{\theta_s}\Delta(z,\theta)P(\theta)\sin(\theta)d\theta\right)}{1+\tau\left(\int_0^{\theta_s} P(\theta)\sin(\theta)d\theta\right)}. \tag{A8}$$

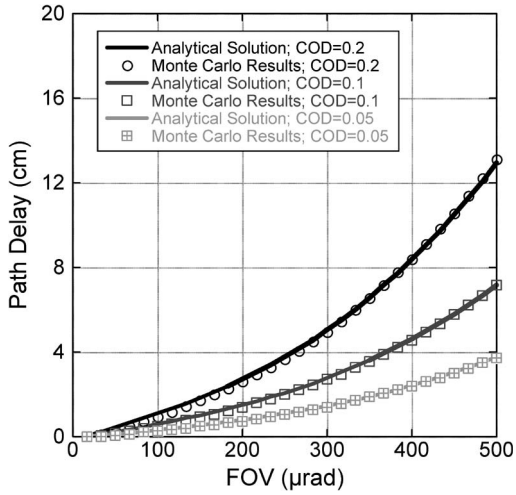

Fig. 11. Comparison of results from the analytical model and the Monte Carlo model with only single scattering. Clouds at 500–1000 m. MODIS phase function for $r_e = 20$ μm used.

If only zeroth- and first-order scatterings are considered, then the contribution of zeroth-order scattering to lidar return is

$$p_{s_0} = \frac{\alpha_s e^{-2\tau}}{\alpha_s e^{-2\tau} + 2\alpha_s \tau e^{-2\tau}\left(\frac{1}{2}\int_0^{\theta_s} P(\theta)\sin(\theta)d\theta\right)} = \frac{1}{1 + 2\tau\left(\frac{1}{2}\int_0^{\theta_s} P(\theta)\sin(\theta)d\theta\right)}. \quad \text{(A9)}$$

As shown in Fig. 4(a), the probability of photons being scattered into the forward-scattering angle range $[0, \theta_s]$, $(1/2)\int_0^{\theta_s} P(\theta)\sin(\theta)d\theta$, is about 50% for a variety of particle sizes and shapes. Approximately, the contribution of zeroth-order scattering can be written as

$$p_{s_0} \approx \frac{1}{1+\tau} \times 100\%. \quad \text{(A10)}$$

Similarly, the contribution of the first-order scattering can be written as

$$p_{s_1} = \left(1 - \frac{1}{1+\tau}\right) \times 100\% = \frac{\tau}{1+\tau} \times 100\%. \quad \text{(A11)}$$

Fig. 11 shows the comparison between the results of this analytical model and our 3-D Monte Carlo model when only single scattering is taken into account. As shown in the figure, these results are essentially identical.

ACKNOWLEDGMENT

The authors would like to thank Drs. C. Chiu, S. Palm, J. Spinhirne, and Z. Zhang for helpful discussions and advice. They would also like to thank the two anonymous reviewers for the helpful comments and suggestions.

REFERENCES

[1] H. J. Zwally, B. Schutz, W. Abdalati, J. Abshire, C. Bentley, A. Brenner, J. Bufton, J. Dezio, D. Hancock, D. Harding, T. Herring, B. Minster, K. Quinn, S. Palm, J. Spinhirne, and R. Thomas, "ICESats laser measurements of polar ice, atmosphere, ocean, and land," *J. Geodyn.*, vol. 34, no. 3/4, pp. 405–445, Oct./Nov. 2002.

[2] D. P. Duda, J. D. Spinhirne, and E. W. Eloranta, "Atmospheric multiple scattering effects on GLAS altimetry—Part I: Calculations of single path bias," *IEEE Trans. Geosci. Remote Sens.*, vol. 39, no. 1, pp. 92–101, Jan. 2001.

[3] E. W. Eloranta, "A practical model for Lidar multiple scattering," *Appl. Opt.*, vol. 37, pp. 2464–2472, 1998.

[4] A. Mahesh, J. D. Spinhirne, D. P. Duda, and E. W. Eloranta, "Atmospheric multiple scattering effects on GLAS altimetry—Part II: Analysis of expected errors in Antarctic altitude measurements," *IEEE Trans. Geosci. Remote Sens.*, vol. 40, no. 11, pp. 2353–2362, Nov. 2002.

[5] J. D. Spinhirne, S. P. Palm, W. D. Hart, D. L. Hlavka, and E. J. Welton, "Cloud and aerosol measurements from GLAS: Overview and initial results," *Geophys. Res. Lett.*, vol. 32, no. 22, p. L22 S03, Sep. 2005. DOI:10.1029/2005GL023507.

[6] Y. Yang, A. Marshak, J. C. Chiu, W. J. Wiscombe, S. P. Palm, A. B. Davis, D. A. Spangenberg, L. Nguyen, J. D. Spinhirne, and P. Minnis, "Retrievals of thick cloud optical depth from the geoscience laser altimeter system (GLAS) by calibration of solar background signal," *J. Atmos. Sci.*, vol. 65, no. 11, pp. 3513–3527, Nov. 2008.

[7] National Research Council, *Earth Science and Applications From Space: National Imperatives for the Next Decade and Beyond*, 2007. Committee on Earth Science and Applications from Space: A Community Assessment and Strategy for the Future, National Research Council, National Academies Press.

[8] J. D. Spinhirne, S. P. Palm, and W. D. Hart, "Antarctica cloud cover for October 2003 from GLAS satellite Lidar profiling," *Geophys. Res. Lett.*, vol. 32, no. 22, p. L22 S05, Sep. 2005. DOI:10.1029/2005GL023782.

[9] R. F. Cahalan, M. McGill, J. Kolasinski, T. Várnai, and K. Yetzer, "THOR—Cloud thickness from offbeam Lidar returns," *J. Atmos. Ocean. Technol.*, vol. 22, no. 6, pp. 605–627, Jun. 2005.

[10] R. F. Cahalan, L. Oreopoulos, A. Marshak, K. F. Evans, A. B. Davis, R. Pincus, K. H. Yetzer, B. Mayer, R. Davies, T. P. Ackerman, H. W. Barker, E. E. Clothiaux, R. G. Ellingson, M. J. Garay, E. Kassianov, S. Kinne, A. Macke, W. O'Hirok, P. T. Partain, S. M. Prigarin, A. N. Rublev, G. L. Stephens, F. Szczap, E. E. Takara, T. Várnai, G. Wen, and T. B. Zhuravleva, "The international intercomparison of 3D radiation codes (I3RC): Bringing together the most advanced radiative transfer tools for cloudy atmospheres," *Bull. Amer. Meteorol. Soc.*, vol. 86, no. 9, pp. 1275–1293, Sep. 2005.

[11] W. Abdalati, R. Bindschadler, C. Carabajal, B. Csatho, M. DiJoseph, J. Dimarzio, H. Fricker, D. Harding, D. Hancock, U. Herzfeld, W. Krabill, R. Kwok, M. Lefsky, T. Markus, A. Marshak, S. Martin, A. Neuenschwander, S. Palm, J. Ranson, B. Schutz, M. Simard, B. Smith, J. Spinhirne, T. Urban, C. Webb, and J. Zwally, *Report of the Ad-hoc Science Definition Team for the Ice Cloud and Land Elevation Satellite-II (ICESat-II)*, 2008. [Online]. Available: https://cires.colorado.edu/~waleed/

[12] B. A. Baum, P. Yang, A. J. Heymsfield, S. Platnick, M. D. King, Y. X. Hu, and S. T. Bedka, "Bulk scattering properties for the remote sensing of ice clouds. Part II: narrowband models," *J Appl. Meteorol.*, vol. 44, no. 12, pp. 1896–1911, Dec. 2005.

[13] P. Yang, H. Wei, H.-L. Huang, B. A. Baum, Y. X. Hu, G. W. Kattawar, M. I. Mishchenko, and Q. Fu, "Scattering and absorption property database for nonspherical ice particles in the near- through far-infrared spectral region," *Appl. Opt.*, vol. 44, no. 26, pp. 5512–5523, Sep. 2005.

[14] S. P. Palm, J. D. Spinhirne, W. D. Hart, and D. L. Hlavka, "GLAS atmospheric data products," *Algorithm Theoretical Basis Document*, 2002, Greenbelt, MD: GSFC. Ver. 4.2. Available: http://www.csr.utexas.edu/glas/pdf/glasatmos.atbdv4.2.pdf

[15] H. J. Zwally, M. A. Beckley, A. C. Brenner, and M. B. Giovinetto, "Motion of major ice-shelf fronts in Antarctica from slant-range analysis of radar altimeter data, 1978–98," *Ann. Glaciol.*, vol. 34, no. 1, pp. 255–262, Jan. 2002.

[16] A. Mahesh, V. P. Walden, and S. G. Warren, "Ground-based infrared remote sensing of cloud properties over Antarctic Plateau. Part II: Cloud optical depths and particle sizes," *J. Appl. Meteorol.*, vol. 40, no. 7, pp. 1279–1294, 2001.

[17] D. L. Mitchell and R. P. d'Entremont, "Satellite remote sensing of small ice crystal concentrations in cirrus clouds," in *Proc. ICCP*, Cancun, Mexico, 2008, pp. 7–11.

[18] R. P. Lawson, B. A. Baker, P. Zmarzly, D. O'Connor, Q. Mo, J.-F. Gayet, and V. Shcherbakov, "Microphysical and optical properties of ice crystals at South Pole Station," *J. Appl. Meteorol. Climatol.*, vol. 45, no. 11, pp. 1505–1524, Nov. 2006.
[19] M. Vaughan, S. Young, D. Winker, K. Powell, A. Omar, Z. Liu, Y. Hu, and C. Hostetler, "Fully automated analysis of space-based Lidar data: An overview of the CALIPSO retrieval algorithms and data products," in Proc. SPIE, Nov. 2004, vol. 5575, pp. 16–30.
[20] E. Weisz, J. Li, W. P. Menzel, A. K. Heidinger, B. H. Kahn, and C.-Y. Liu, "Comparison of AIRS, MODIS, CloudSat and CALIPSO cloud top height retrievals," *Geophys. Res. Lett.*, vol. 34, no. 17, p. L17 811, Sep. 2007. DOI:10.1029/2007GL030676.
[21] M. J. Pavolonis and J. R. Key, "Antarctic cloud radiative forcing at the surface estimated from the AVHRR Polar pathfinder and ISCCP D1 datasets, 1985–93," *J. Appl. Meteorol.*, vol. 42, no. 6, pp. 827–840, Jun. 2003.
[22] A. Heymsfield, "Properties of tropical and midlatitude ice cloud particles ensembles. Part II. Applications for mesoscale and climate models," *J. Atmos. Sci.*, vol. 60, no. 21, pp. 2592–2611, Nov. 2003.
[23] G. E. Thomas and K. Stamnes, *Radiative Transfer in the Atmosphere and Ocean*, vol. 517. Cambridge, U.K.: Cambridge Univ. Press, 1999, p. 1999.
[24] P. Yang, G. W. Kattawar, G. Hong, P. Minnis, and Y. Hu, "Uncertainties with the surface of ice particles in satellite-based retrieval of cirrus clouds: Part I. Single-scattering properties of ice crystals with surface roughness," *IEEE Trans. Geosci. Remote Sens.*, vol. 46, no. 7, pp. 1940–1947, Jul. 2008.
[25] A. Mahesh, M. A. Gray, S. P. Palm, W. D. Hart, and J. D. Spinhirne, "Passive and active detection of clouds: Comparisons between MODIS and GLAS observations," *Geophys. Res. Lett.*, vol. 31, no. 4, p. L04 108, Feb. 2004. DOI:10.1029/2003GL018859.
[26] C. Naud, J.-P. Muller, and P. de Valk, "On the use of ICESAT–GLAS measurements for MODIS and SEVIRI cloud-top height accuracy assessment," *Geophys. Res. Lett.*, vol. 32, no. 19, p. L19 815, Oct. 2005. DOI:10.1029/2005GL023275.

Yuekui Yang received the B.S. and M.S. degrees in atmospheric sciences from the Science and Engineering University of the Army, Nanjing, China, in 1987 and 1990, respectively, and the Ph.D. degree in atmospheric sciences from the University of Illinois at Urbana–Champaign, in 2007.

From 1990 to 1997, he was a Research Scientist with the Aviation Meteorological Research Institute, Beijing, China. From 1997 to 1999, he was a Software Engineer with Beijing METSTAR Radar Company, Ltd. From 1999 to 2001, he was a Project Manager with the Datatrust Information Technologies, Beijing. Since 2007, he has been with the Goddard Earth Sciences and Technology Center, University of Maryland, Baltimore County, Baltimore. His research experience includes radiative-transfer modeling, satellite cloud detection, and study on polar clouds and blowing snow with both passive and active remote-sensing instruments.

Alexander Marshak received the M.S. degree in applied mathematics from Tartu University, Tartu, Estonia, in 1978 and the Ph.D. degree in numerical analysis from the Academy of Sciences of the USSR, Novosibirsk, Russia, in 1983.

In 1978, he joined the Institute of Astrophysics and Atmospheric Physics, Estonia, where he worked for 11 years. In 1989, he received an Alexander von Humboldt fellowship and worked for two years with Göttingen University, Göttingen, Germany. In 1991, he joined Goddard Space Flight Center (GSFC), first working for SSAI, then UMBC/JCET, and finally, NASA/GSFC, where he has been since 2003. He has published over 100 refereed papers, books, and chapters in edited volumes.

Tamás Várnai received the M.S. degree equivalent diploma in meteorology from Eötvös Loránd University, Budapest, Hungary, in 1989 and the Ph.D. degree in atmospheric and oceanic sciences from McGill University, Montreal, QC, Canada, in 1996.

From 1989 to 1991, he was Research Scientist with the Hungarian Meteorological Service. From 1997 to 1999, he was a Postdoctoral Fellow with the University of Arizona, Tucson. In 1999, he moved to the Joint Center for Earth System Technology of the University of Maryland, Baltimore County, Baltimore, and of the NASA Goddard Space Flight Center, Greenbelt, MD, where he is currently a Research Associate Professor of Physics. His research interests focus on 3-D radiative processes in clouds and on remote sensing of cloud properties.

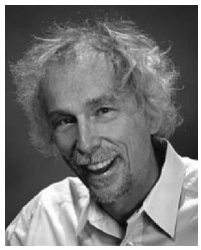

Warren Wiscombe received the B.S. degree in physics from Massachusetts Institute of Technology, Cambridge, in 1964 and the M.S. degree in physics and the Ph.D. degree in applied mathematics from the California Institute of Technology, Pasadena, in 1966 and 1970, respectively.

From 1969 to 1975, he was a Research Scientist with Systems, Science and Software, La Jolla, CA. From 1974 to 1980, he was a Staff Scientist with the National Center for Atmospheric Research. From 1980 to 1984, he was an Associate Professor with the Department of Applied Sciences, New York University, New York. Since 1984, he has been with NASA Goddard Space Flight Center, Greenbelt, MD, where he joined as a Senior Research Scientist. He is currently also the Chief Scientist of Department of Energy's Atmospheric Radiation Measurement (ARM) Program and an Adjunct Professor with the University of Maryland, Baltimore. His research covers radiative transfer, light scattering, cloud radiation, climate theory, remote sensing, and science data systems.

Dr. Wiscombe has been a Fellow of American Meteorological Society since 1989.

Ping Yang received the B.S. degree in theoretical physics from Lanzhou University, Lanzhou, China, in 1985, the M.S. degree in atmospheric physics from Lanzhou Institute of Plateau Atmospheric Physics, Chinese Academy of Sciences, Lanzhou, in 1988, and the Ph.D. degree in meteorology from the University of Utah, Salt Lake City, in 1995.

After graduation from the University of Utah, he remained there for two years, where he worked as a Research Associate. He was an Assistant Research Scientist with the University of California at Los Angeles and an Associate Research Scientist with the Goddard Earth Sciences and Technologies Center, University of Maryland, Baltimore. He is currently a Professor with the Department of Atmospheric Sciences, Texas A&M University, College Station, where he also has a joint professor appointment with the Department of Physics. His research interests are in the areas of remote sensing and radiative transfer. He has been actively conducting research in the modeling of the optical and radiative properties of clouds and aerosols, particularly cirrus clouds, and their applications to spaceborne and ground-based remote sensing. He has coauthored more than 140 peer-reviewed publications. He currently serves as an Associate Editor for the *Journal of Atmospheric Sciences*, the *Journal of Quantitative Spectroscopy and Radiative Transfer*, and the *Journal of Applied Meteorology and Climatology*. He is a member of the MODIS Science Team.

Dr. Yang was the recipient of the Best Paper Award from the Climate and Radiation Branch, NASA Goddard Space Center in 2000, the U.S. National Science Foundation CAREER award in 2003, and the Dean's Distinguished Achievement Award for Faculty Research, College of Geosciences, Texas A&M University in 2004.